Available online at www.sciencedirect.com
SCIENCE DIRECT®
Journal of Solid State Chemistry 179 (2006) 2111–2119
JOURNAL OF SOLID STATE CHEMISTRY
www.elsevier.com/locate/jssc

Structural and ^{31}P NMR investigation of $Bi(MM')_2PO_6$ statistic solid solutions: Deconvolution of lattice constraints and cationic influences

Marie Colmont[a], Laurent Delevoye[a], El Mostafa Ketatni[b], Lionel Montagne[a], Olivier Mentré[a,*]

[a]Laboratoire de cristallochimie et physicochimie du solide de Lille—UMR CNRS N° 8012—ENSCL, BP 108–59650 Villeneuve d'Ascq, France
[b]Laboratoire de Spectro-Chimie Appliqué et Environnement, Faculté des Sciences et Techniques, BP 523, Béni Mellal, Morocco

Received 16 February 2006; received in revised form 31 March 2006; accepted 2 April 2006
Available online 25 April 2006

Abstract

Two solid solutions $BiM_xMg_{(2-x)}PO_6$ (with M^{2+} = Zn or Cd) have been studied through ^{31}P MAS NMR. The analysis has been performed on the basis of refined crystal structures through X-ray diffraction and neutron diffraction. The $BiZn_xMg_{(2-x)}PO_6$ does not provide direct evidence for sensitive changes in the phosphorus local symmetry. This result is in good agreement with structural data which show nearly unchanged lattices and atomic separations through the Zn^{2+} for Mg^{2+} substitution. On the other hand, the Cd^{2+} for Mg^{2+} substitution behaves differently. Indeed, up to five resonances are observed, each corresponding to one of the five first-cationic neighbour distributions, i.e. 4Mg/0Cd, 3Mg/1Cd, 2Mg/2Cd, 1Mg/3Cd and 0Mg/4Cd. Their intensities match rather well the expected weight for each configuration of the statistical Cd^{2+}/Mg^{2+} mixed occupancy. The match is further improved when one takes into account the influence of the 2nd cationic sphere that is available from high-field NMR data (18.8 T). Finally, the fine examination of the chemical shift for each resonance versus x allows to de-convolute the mean Z/a^2 effective field into two sub-effects: a lattice constraint-only term and a chemical-only term whose effects are directly quantifiable.
© 2006 Elsevier Inc. All rights reserved.

Keywords: Bismuth oxyphosphate; ^{31}P solid-state NMR; Neutron diffraction

1. Introduction

In the course of the investigation of mixed Bi^{3+}/M^{2+} phosphate oxides, a great number of new materials that display new related structural types have been discovered and show fascinating structural relationships [1–7]. As detailed in a previous study, a common description can be used, which evidences the framework based on infinite polycationic ribbons of formula $[M_4Bi_{2n-2}O_{2n}]^{(2+2n)+}$, where n stands for the number of tetrahedra along the variable size [8]. These ribbons are built from fluorite-like edge-sharing $O(Bi,M)_4$ tetrahedra and are surrounded by isolated phosphate groups. Within a structural approach, based on DRX analyses, the materials have been classified as "ordered" or "disordered" depending on the chemical nature of the edges of the ribbons. Ordered compounds such as $BiMPO_5$ (M = Co, Ni, Mn…) [9–12] or BiM_2PO_6 (M = Cu, Mg, Zn, Cd, Pb…) [6,7,13–16] show a regular cationic periodicity inside the ribbons. For instance, in the latter compound, $[M_2Bi_1O_2]^{3+}$ 2-tetrahedra wide ribbons (= D), Bi^{3+} are solely located at the centre of the ribbons while M^{2+} occupy the edges in an ordered manner. On the opposite, any disordered compounds still contain Bi^{3+} at their centres but mixed Bi^{3+}/M^{2+} positions at their edges. As a matter of fact, the disorder is reflected on neighbouring PO_4 groups, which bond the edges [2–4]. The structural resolution using either neutron or X-ray source shows the superimposition of multi-oriented PO_4 around the central phosphorus atom in the average unit cell. Considering the disordered phases, both X-ray diffraction (XRD) and solid ^{31}P NMR appear complementary in order to view (1) either discrete or continuous orientation of PO_4 in disordered materials, and (2) the correlation of their close coordination sphere with the ^{31}P nuclei chemical shift.

*Corresponding author. Fax: +33 320436814.
E-mail address: mentre@ensc-lille.fr (O. Mentré).

0022-4596/$ - see front matter © 2006 Elsevier Inc. All rights reserved.
doi:10.1016/j.jssc.2006.04.014

The first stage of a spectroscopic NMR investigation applied to PO_4 groups within such complex structural edifices must be preceded by a preparative work on expected chemical shifts occurring in "ordered" compounds. In these latter compounds, PO_4 environments are roughly comparable. Thus, the accurate assignment of isolated resonances appears necessary for the consideration of the various influent structural factors. Indeed, it is well known that the NMR chemical shift of a given nucleus X is sensitive to the local environment related to a number of factors including the geometries of the anionic X–O and cationic X–M coordination spheres that combine in the local electrostatic field. For the specific case of ^{31}P NMR, the second-order cationic sphere is essential since within these series of related materials, the tetrahedral PO_4 geometry may remain nearly unchanged. Hence, a pertinent set of cationic substitution may help to distinguish between competing effects. For instance, in the case of a solid solution, one should assume that the local geometry is ruled out by an averaging effect, which is locally undergone by each cation in term of either geometric constraints or geometric relaxations, depending on the cationic size of the substituted species. Consequently, the NMR local probe helps to separate, in the most appropriate cases, the competing origins of the chemical shifts. Furthermore, the quantitative feature of NMR can be very informative compared to XRD precision especially in the case of poor cationic contrast. For example, it can provide informations about pure statistical distribution, possible cationic segregation or even ordering. The choice for $BiZn_xMg_{2-x}PO_6$ and $BiCd_xMg_{2-x}PO_6$, the two solid solution systems investigated in this work, was driven by the fact that the influences of the mean electrostatic fields for Zn^{2+} and Mg^{2+} are comparable, whereas the influences of Cd^{2+} and Mg^{2+} are drastically different. The comparison of XRD/neutron diffraction (ND) analysis with NMR results was developed as far as possible.

So far, equivalent studies on various solid solution systems [17–19] essentially yield to quantitatively establish or confirm the nature of the cationic distribution, e.g. statistic in $Zn_{3-x}Mg_x(PO_4)_2$ [20]. In addition, the work presented here focuses on the fine interpretation of the chemical shift origin. No examples were found for the use of NMR in the investigation of Cd versus Mg systems. However, our interest was reinforced by the weaker electrostatic field that characterizes the former cation ($\propto Z_{\mathrm{eff}}/a^2$, as explained in the discussion).

2. Experimental

Synthesis: Pure $BiZn_xMg_{2-x}PO_6$ and $BiCd_xMg_{2-x}PO_6$ compounds were prepared from stoichiometric mixtures of $(NH_4)_2HPO_4$, ZnO, CdO, MgO and Bi_2O_3. After grinding in an agate mortar, the powders were heated up to 800 °C for 24 h. Several intermediate steps were necessary between 200 and 500 °C to facilitate the removal of volatile species.

Diffraction: XRD analyses have been performed on a Siemens D-5000 diffractometer (θ–2θ geometry, back monochromatized, λ Cu-$K\alpha$ radiation). ND data have been collected on the D1a diffractomeer at the Institut Laue Langevin (ILL), Grenoble, France, $\lambda = 1.909$ Å. The Rietveld refinements described below have been performed using Fullprof 2000 [21].

^{31}P NMR spectroscopy: Solid-state magic angle spinning (MAS) ^{31}P NMR spectra of the prepared materials were obtained on a Bruker AV400 at a resonant frequency of 161.98 MHz, at MAS speeds of 10 kHz (4 mm MAS probe) and 28 kHz (2.5 mm MAS probe) and on a Bruker AV800, working at resonant frequency of 323.87 MHz, at a MAS speed of 25 kHz (2.5 mm MAS probe). The ^{31}P nucleus (spin $I = 1/2$) is sensitive to both chemical shift and dipolar interactions, which are reduced to the isotropic value for the chemical shift interaction and to zero for the dipolar interaction under MAS. The high spinning speeds (25 and 28 kHz) were used to ensure that the remaining ^{31}P broadening was not due to strong dipolar couplings. The spectra at 161.98 MHz were recorded using a single pulse of 0.8 μs ($\pi/8$), with 5 s recycle delays, and 128 scan averages. At 323.87 MHz, the pulse excitation was 1.5 μs ($\pi/8$), the recycle delay was 20 s and 32 scans were used for signal averaging. The optimization of the recycle delays have been experimentally checked to ensure full T_1 relaxation in between scans. The spectra were referenced to external phosphoric acid ($\delta = 0$ ppm). The relative intensity of the different peaks was deduced from a deconvolution using the DMfit program [22].

3. Structural analysis

Priory to the ^{31}P NMR resonance assignment, it is worth examining carefully the symmetries and local environments for the investigated systems.

Lattice parameters: Fig. 1a shows the least-squares refined lattice parameters for $BiZn_xMg_{2-x}PO_6$ and $BiCd_xMg_{2-x}PO_6$. These parameters remain nearly constant for the former and show drastic changes versus x for the latter. The volume unit cell variation is in good agreement with the ionic radii, $r\ Zn^{2+}(V) = 0.68$ Å, $r\ Mg^{2+}(V) = 0.66$ Å, $r\ Cd^{2+}(V) = 0.87$ Å [23]. These cationic characteristics are at the basis of our choice for the two systems used in the ^{31}P NMR investigation. The crystal structure of BiM_2XO_6 materials projected along the b-axis is shown in Fig. 1b, highlighting the double ribbon (D) surrounded by PO_4.

Symmetry ambiguity and structural refinement: For these series of BiM_2PO_6 compounds, an ambiguity on the real space group (SG) has already been pointed out [15]. The PO_4 rotation that can bring PO_4 out of symmetry elements may generate a symmetry lowering compared to that of the Bi–M–O framework. The reported SG at room temperature are generally either *Pnma*, or *Bbmm*. In the $BiMg_2VO_6$ case [24], the centring displacive transition from one form to another at 350 K, clearly shows the difficulty to establish

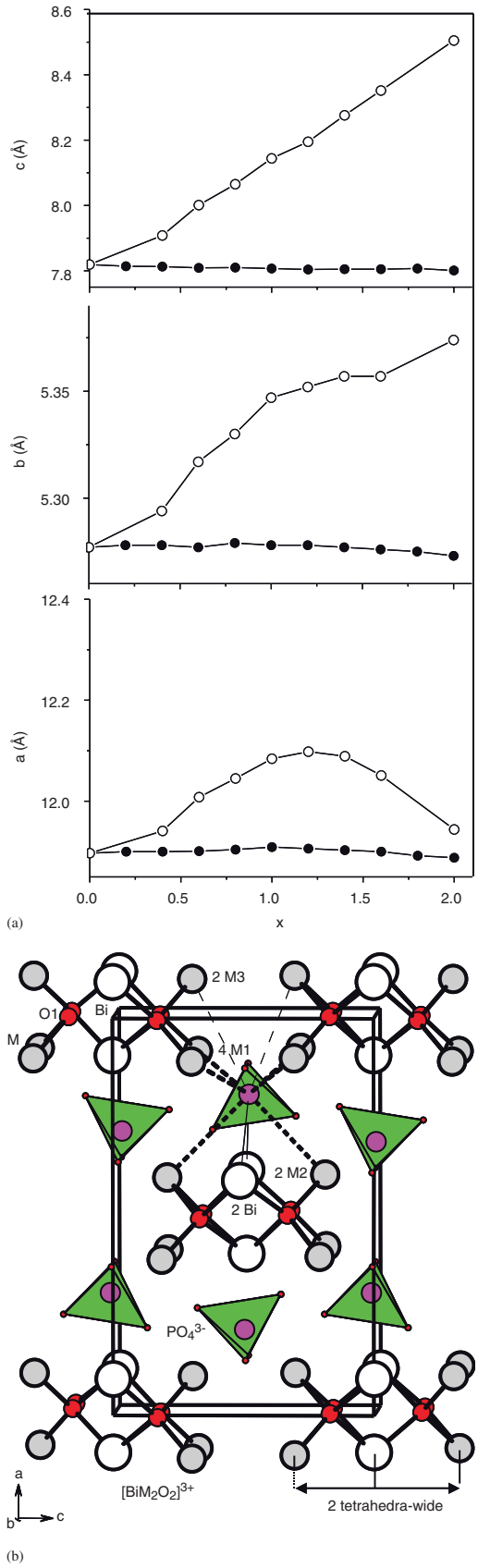

Fig. 1. Lattice parameters versus x for $BiZn_xMg_{(2-x)}PO_6$ (full circles) and $BiCd_xMg_{(2-x)}PO_6$ (empty circles): (a) projection along the b axis of the BiM_2PO_6 crystal structure; (b) bonding scheme of the phosphorus atom.

true space groups from powder XRD, while ND is more relevant because of its great sensitivity to oxygen accurate locations, e.g. the ND reexamination of $BiMg_2PO_6$ [25] yields the *Pnma* SG instead of the previously announced *Bbmm* from powder Rietveld refinement [6]. Thus, announced materials with B-centring SG are possibly doubtful. However, from the point of view of crystallography, the number of independent phosphorus positions remained unchanged in the two SG while in addition to the common O(1) atom, the two independent oxygen atoms form the XO_4 tetrahedron in *Bbmm* (O(2) + O(3) with multiplicities 2 + 2) versus three independent oxygen atoms in *Pnma* (O(2) + O(3) + O(4) with multiplicities 2 + 1 + 1). For the Rietveld analyses of the Zn/Mg compounds, a second minor phase, present as an impurity, was introduced in the refinement process. It corresponds to the recently reported disordered $Bi_{\sim1.2}M_{\sim1.2}PO_{5.5}$ with parameters $a\sim14.8$ Å, $b\sim11.2$ Å, $c\sim5.4$ Å, SG Ibam [8]. In any case, the M^{2+} sites were filled with the correct M/M' ratio. It leads to acceptable values of thermal parameters for all atoms, in good agreement with a M/M' statistic distribution. However, M and M' partial segregation without long-range ordering cannot be totally excluded and would not be quantified by XRD techniques whereas a local investigation using NMR spectroscopy appears well adapted to this problematic.

Phosphorus environment: The mean phosphorus surrounding atomic shell is highlighted in Fig. 1b with the atomic labelling used above. For $BiCd_xMg_{2-x}PO_6$, the crystal structures were refined through XRD data in the apparent *Bbmm* SG. Data for $BiCd_2PO_6$ were taken from Ref. [26]. The pertinent results concerning our study are tabulated in Tables 1 and 2. For the $BiZn_xMg_{2-x}PO_6$ solid solution, the crystal structure was refined through ND data. The symmetry lowering from *Bbmm* to *Pnma* is evidenced by the observation of 201 and 011 reflections on the ND patterns, Fig. 2. In the Zn-rich domain, it is directly observable on XRD patterns. The mean P–O distance roughly follows the evolution of the lattice parameters, i.e. nearly unchanged (~1.5 Å) versus x along the Zn to Mg substitution, and is in the 1.39 Å $< d <$ 1.56 Å range for Cd/Mg compounds. Two P–M^{2+} shells can be distinguished up to 4 Å: four shorter P–$M1$ and two longer P–$M2$. For the *Pnma* space group, note the splitting in two P–$M1a$/2 P–$M1b$ and one P–$M2a$/P–$M2b$ with sensitive changes in the two antagonist P–$M2$ separations. Two bismuth cations also surround the central phosphorus cation with P–Bi distances that are included within the 3.6–3.8 Å range.

4. NMR spectroscopy

The ^{31}P MAS NMR spectra for the two solid solutions are presented in Fig. 3. In the case of a Zn^{2+}/Mg^{2+} substitution, there is an additional weak resonance which is attributed to an impurity, cf. the XRD analysis.

Table 1
Refinement parameters and selected distances (Å) for $BiZn_xMg_{2-x}PO_6$ (SG *Pnma*)

x	0[a]	0.8[b]	1.2[b]	1.4[b]	1.6[b]	2[c]
a (Å)	11.8948(3)	11.8947(3)	11.8903(2)	11.8893(3)	11.8888(2)	11.8941(3)
b (Å)	5.2743(1)	5.2722(1)	5.2723(1)	5.2726(1)	5.2723(1)	5.2754(2)
c (Å)	7.8088(2)	7.7956(2)	7.7999(2)	7.8033(2)	7.8052(2)	7.8161(2)
R_F (%)	2.3	7.22	4.39	4.16	2.43	3.80
R_B (%)	—	6.31	4.53	4.47	2.65	5.64
χ^2	—	8.90	4.58	3.20	2.18	4.49
P–O(2) × 2	1.569	1.537	1.547	1.540	1.537	1.56
P–O(3)	1.431	1.510	1.542	1.530	1.516	1.44
P–O(4)	1.566	1.551	1.508	1.526	1.530	1.43
$\overline{P-O}$	1.53	1.53	1.54	1.53	1.53	1.50
P–$M1a$ × 2	3.295	3.278	3.315	3.310	3.309	3.295
P–$M1b$ × 2	3.286	3.269	3.233	3.239	3.239	3.224
P–$M2a$	3.415	3.528	3.509	3.509	3.497	3.556
P–$M2b$	3.440	3.333	3.292	3.299	3.288	3.306
P–Bi × 2	3.592	3.598	3.588	3.592	3.594	3.612
$\overline{M-O}$ × 5	2.02	2.02	2.03	2.04	2.05	2.07
$\overline{Bi-O}$ × 4	2.20	2.19	2.21	2.20	2.20	2.32

[a]XRD single crystal data from Ref. [6].
[b]Neutron diffraction data.
[c]Powder XRD data from Ref. [15].

Table 2
Refinement parameters and selected distances (Å) for $BiCd_xMg_{2-x}PO_6$

x	0[a]	0.6[b]	1[b]	1.6[b]	2[c]
a (Å)	11.8948(3)	12.0103(5)	12.0854(3)	12.0488(4)	11.9421(2)
b (Å)	5.2743(1)	5.3162(2)	5.3452(1)	5.3588(2)	5.3728(1)
c (Å)	7.8088(2)	8.0013(4)	8.1424(2)	8.3572(2)	8.5026(1)
R_F (%)	2.3	3.64	5.25	4.68	7.0
R_B (%)	—	5.35	7.85	5.81	8.2
χ^2	—	1.57	1.76	1.50	2.3
P–O(2) × 2	1.569	1.426	1.539	1.442	1.422
P–O(3) × 2	1.431/1.566	1.533	1.393	1.351	1.467
$\overline{P-O}$	1.53	1.50	1.47	1.40	1.44
P–$M1$ × 4	3.295/3.286	3.294	3.286	3.312	3.301
P–$M2$ × 2	3.415/3.440	3.403	3.481	3.524	3.605
P–Bi × 2	3.592	3.631	3.717	3.724	3.760
$\overline{M-O}$ × 5	2.02	2.11	2.14	2.22	2.24
$\overline{Bi-O}$ × 4	2.20	2.22	2.29	2.26	2.28

[a]XRD single crystal data from Ref. [6],—SG *Pnma*.
[b]Powder XRD data—SG *Bbmm*.
[c]Powder XRD data from Ref. [26]—SG *Bbmm*.

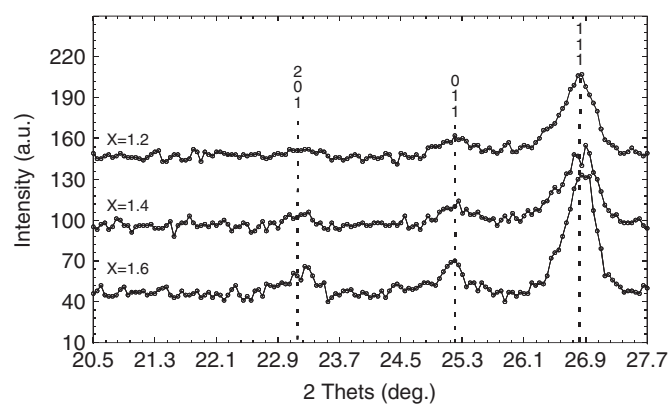

Fig. 2. Neutron diffraction patterns of $BiZn_{1.2}Mg_{0.8}PO_6$, $BiZn_{1.4}Mg_{0.6}PO_6$, $BiZn_{1.6}Mg_{0.4}PO_6$ with evidence of the B-centring violation.

Let us first consider the three border compositions. Each compound shows a single narrow resonance of ca. 2 ppm broad at the following chemical shifts: −7.33 ppm for $BiMg_2PO_6$, −3.77 ppm for $BiZn_2PO_6$ and 12.6 ppm for $BiCd_2PO_6$.

A good correlation of ^{31}P solid-state NMR results of powdered samples with structural information about the bonding of phosphate groups can be obtained through the analysis of the chemical shift anisotropy [27–29]. However, orthophosphates show a small anisotropy (15–20 ppm) and the correlation mentioned in Ref. [27] is difficult to obtain due to the overlapping of several resonances, as shown in Fig. 3b. The CSA amplitude has been determined for the Cd/Mg system using ^{31}P spectra obtained at a slow MAS speed (5 kHz), but the results show no significant change (15–16 ppm) versus the x. Another possibility for the correlation of NMR results with structural data is to consider that the variation of ^{31}P chemical shift is mainly due to the influence of the first-neighbour cationic shell rather than to oxygen ligands. Previous NMR studies [27–29] have reported in various series of orthophosphate compounds, the linear dependency of the chemical shift with (i) the electronegativity, (ii) the Z/r or (iii) the Z/r^2, where Z is the atomic number and r the atomic radius of the first-neighbour cation.

In the present work, because of our interest in the cationic shell effect, we will correlate the experimental ^{31}P chemical shift with the electric field strength $F = Z/a^2$ for

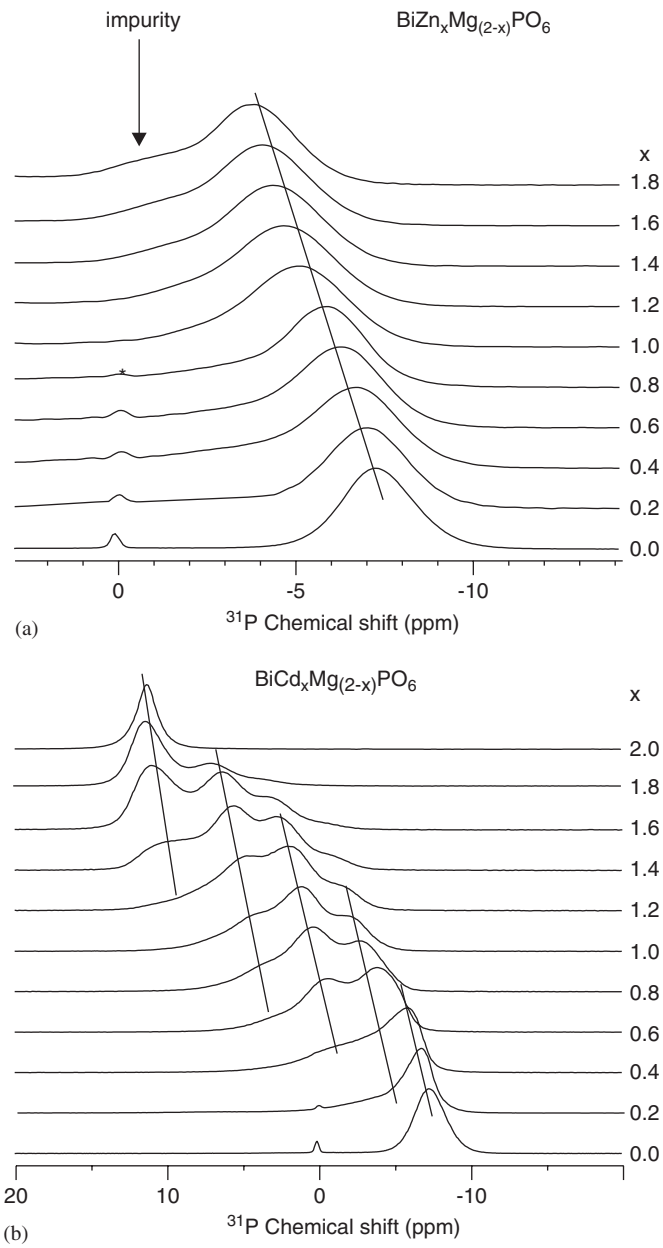

Fig. 3. ^{31}P spectra of (a) $BiZn_xMg_{(2-x)}PO_6$ and (b) $BiCd_xMg_{(2-x)}PO_6$ solid solutions. The fraction of zinc and magnesium on one hand, and of cadmium and magnesium on the other hand is defined by the value x ($0<x<2$). The symbol $*$ denotes the presence of an impurity in the compound. The spectra were obtained at 9.4 T (resonant frequency of 161.98 MHz) at a MAS speed of 10 kHz.

a given M neighbouring cation; here, Z is the valency, and a is the internuclear distance M–O. The shift versus tabulated Z/a^2 [30] are presented in Fig. 4 and shows a good correlation. Indeed, Z/a^2 intrinsically describes two cooperative origins of these modifications, i.e. (a) the lattice constraints arising from geometrical effects in the crystal, (b) the chemical effects that depend on the nature of a given neighbour (efficient through its electronic configuration, electronegativity, polarizability…). One of the key goals of our work was to estimate the relative weight of each effect through cationic substitution.

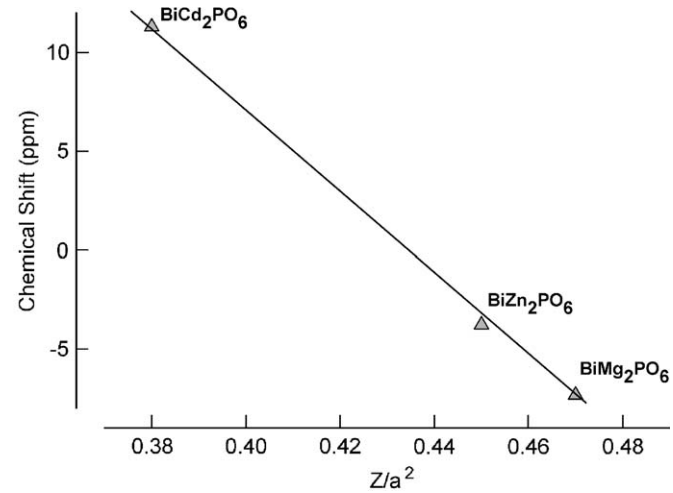

Fig. 4. Variation of the experimental ^{31}P chemical shift versus the cation field strength as defined in the text.

The $BiZn_xMg_{2-x}PO_6$ system: As expected from the close Z/a^2 values for the two antagonist cations, the variation of the chemical shift is weak and monotone between the two end-members. The results of Table 1 indicate no significant changes of the lattice parameters and of the $\overline{P-O}$ bonds. The δ-variation is *mainly due* to a slight decrease of the covalent character of M–(OPO_3) bonds versus increasing x. Considering that a single resonance is observed, we conclude that Zn^{2+} and Mg^{2+} induce comparable lattice constraints in the $[BiPO_6]^{2-}$ framework and thus, Z/a^2 appears as the most appropriate way to distinguish Zn^{2+} from Mg^{2+}, from the ^{31}P NMR point of view.

The $BiCd_xMg_{2-x}PO_6$ system: On the other hand, the Cd/Mg substitution is associated with strong variations of both the ^{31}P chemical shift and the effective field Z/a^2. The examination of the crystal structure reveals a large unit cell volume increase versus x. This phenomenon is especially marked by $\overline{P-O}$ (from 1.53 to 1.44 Å) decrease and $\overline{M-O}$ (from 2.02 to 2.24 Å) increase while the first cationic shell around P remains nearly unchanged ($\overline{P-M1}$~3.3 Å all along the solid solution), Table 2. Thus, it is rather clear that because of their radii, larger Cd^{2+} species locally undergo lattice constraints that are imposed by the smaller Mg^{2+}, while this latter undergoes relaxed effects.

Even though crystallographic data reveal the presence of a unique phosphate group within the structure, we observe an important modification of the ^{31}P MAS spectrum as Cd^{2+} is substituted to Mg^{2+}. Indeed, ^{31}P spectra represent the modification of the local environment of a phosphate, and the different resonances can be associated to the possible Cd/Mg combination within the first cationic shell. In addition to the shorter P–$M1$ distances compared to P–$M2$, the first shell plays a particular role toward phosphates since each O(2) corners bond two $M1$ sites of the cationic shell while the O(3) corners only bond one $M2$ cation. This should lead to a predominant shielding

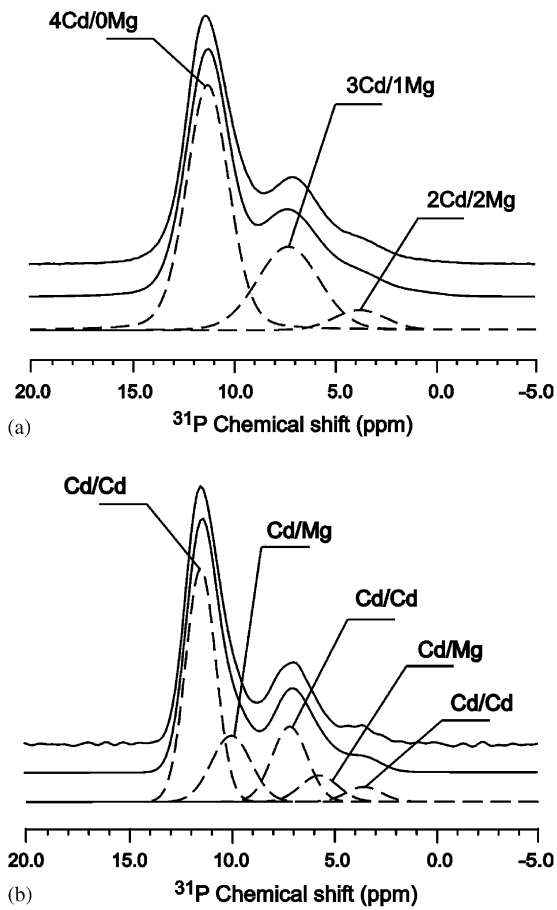

Fig. 5. ^{31}P MAS NMR spectra (top) of $BiCd_{1.8}Mg_{0.2}PO_6$ at 9.4 T (left) and 18.8 T (right) together with the individual lineshapes (bottom) resulting from the de-convolution of the spectra. Gaussian lineshapes were used for the deconvolution of the spectrum with a small Lorentzian contribution (less than 20%). The MAS speeds were set to 28 kHz (9.4 T) and 25 kHz (18.8 T).

influence on phosphorus nuclei. Hence, in a first approximation, there are five different sets of cationic surroundings within a sphere of 3.3 Å: 4Mg/0Cd, 3Mg/1Cd, 2Mg/2Cd, 1Mg/3Cd and 0Mg/4Cd, which are therefore represented by a maximum of 5 resonances on the ^{31}P spectra. Each ^{31}P spectrum of the solid solution was de-convoluted using a series of Gaussian lines using DMfit program [22]. Such an example of de-convolution is shown in Fig. 5 for the $BiCd_{1.8}Mg_{0.2}PO_6$. As Cd is present in majority within this compound, we considered the three most probable configurations (4Cd/0Mg, 3Cd/1Mg and 2Cd/2Mg) out of the five possible ones. The same de-convolution process is applied to each compound of the solid solution; this process leads to informative data about both the intensity of each peak and the associated chemical shift.

5. Results and discussion

Statistic Mg^{2+}/Cd^{2+} occupancies: The relative area of each 1st shell configuration is plotted against the composition in Fig. 6 (left column—triangles). For a statistic cation distribution across all four sites, the intensities of the five resonances should be proportional to the binomial probability of each of the five possible PO_4 environments to occur. The theoretical probability to find the configuration $(Cd_yMg_{4-y})_{1st\ shell}$ around a phosphate in the $BiCd_xMg_{2-x}PO_6$ compound is given by

$$P[Cd_yMg_{4-y}] = C_4^y(2-x)^{4-y}(x)^y,$$

where $C_4^y = 4!/y!(4-y)!$.

In Fig. 6 (left column, lines), this theoretical probability is given for each configuration as a function of x (full line). The linewidths for individual components are included in the 2.5–4 ppm range. One can see that the experimental results fit well the theoretical probability curve. This confirms the random nature of the Cd/Mg cation substitution while diffraction results could not reject the possibility of partial segregation within the lattice, for various chemical reasons.

Influence of the second cationic shell: It is sometimes possible to see on Fig. 6 a certain amount of deviation between the experimental points and the theoretical model. This encouraged us to consider the possibility of *second-neighbour* effects. Such an approach has been adopted by Jakeman et al. [20] with the solid solution $Zn_{3-x}Mg_x(PO_4)_2$ for which an excellent resolution of the ^{31}P MAS spectra was obtained. In our case, an improvement of the resolution was obtained using a very high static field (18.8 T) instead of the more conventional 9.4 T. By comparing Fig. 5a (9.4 T) and 5b (18.8 T), specifically for the composition $BiCd_{1.8}Mg_{0.2}PO_6$, it is possible to observe that a perfect de-convolution requires the addition of several resonances, which are notably revealed by a shoulder around 12 ppm on the right of the main resonance. This effect can be assigned to second-neighbour contributions. It is noteworthy that our attempts to neglect second-neighbour contributions led to strong residual difference-plots. The correct fit of the 18.8 T spectrum involves five resonances instead of three at 9.4 T. Considering the two P–*M*2 influence (3.4–3.6 Å), each 1st shell contribution can be split into three sub-resonances (Cd/Cd, Cd/Mg and Mg/Mg) as schematized in Fig. 7 for the $BiCd_{1.8}Mg_{0.2}PO_6$. The expected weight of the $(Cd_yMg_{4-y})_{1st\ shell}$ with the $(Cd_{2-y'}Mg_{y'})_{2nd\ shell}$ in the $BiCd_{2-x}Mg_xPO_6$ compound is given by

$$P[Cd_yMg_{4-y}] \times P'[Cd_yMg_{2-y'}] = [C_4^y(2-x)^{4-y}(x)^y] \times [C_2^{y'}(2-x)^{2-y'}x^{y'}],$$

where $C_4^y = 4!/y!(4-y)!$ and $C_2^{y'} = 2!/y'!(4-y')!$.

The resonances with a theoretical intensity lower than 4% are not considered in the fit. However, a separation of shift between second neighbours contribution of about 1.4 ppm is considered. The individual linewidths are now within a more realistic range of 1.7–2 ppm. Finally, for all the compositions the spectra have been re-deconvoluted

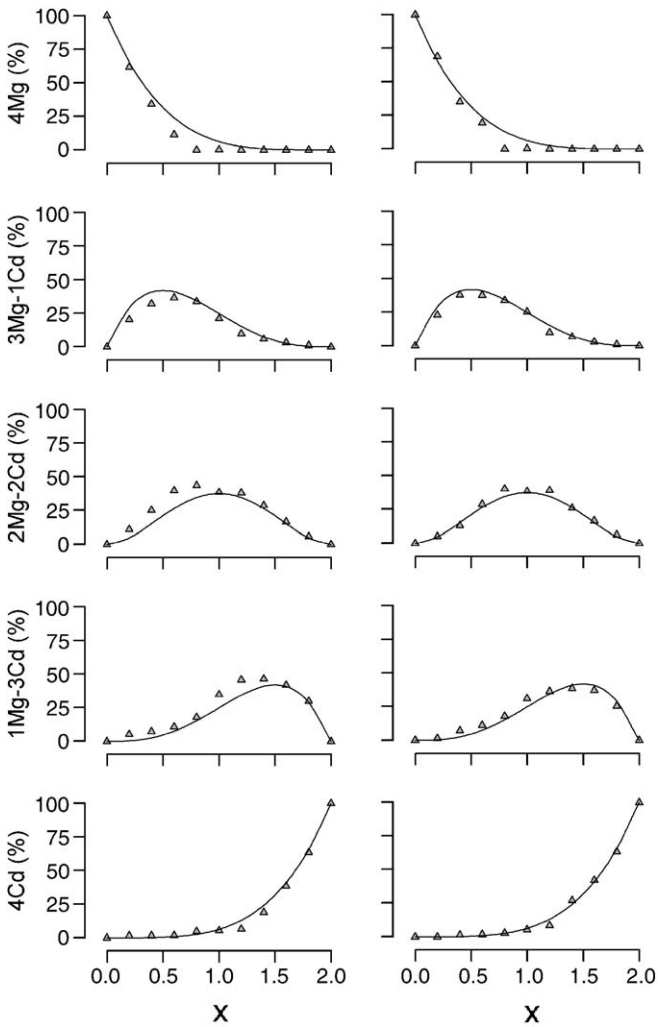

Fig. 6. Experimental (grey triangles) and calculated (full line) variations of the intensity of ^{31}P resonances versus the substitution rate x. The curves are given for each possible configuration of cations. Left column: influence of *first-neighbour* cations only. Right column: *first-neighbour* and *second-neighbour* cations.

taking account of the second neighbour effects. A separation of 1.4 ppm between the satellite peaks with $I > 5\%$ as the existence criterion. The contribution of the 1st cationic shell calculated by the sum of the sub-peaks contribution is plotted against the theoretical values in Fig. 6b (right column) showing a better matching.

Chemical shift analysis: Fig. 8 shows the ^{31}P chemical shift against x for each $[Cd_{4-x}Mg_x]_{1st\ shell}$ configuration. The five series of points roughly follow the same linear evolution. The mean Z/a^2 effect between $BiCd_2PO_6$ and $BiMg_2PO_6$ is pictured by the dotted line between the two extreme points. Here, it is clear that the two combined effects fully describe Z/a^2, i.e. $1-a$ vertical translation that describes a given structural geometry, the influence of the cationic nature, and two-configuration lines that show the influence of the lattice distortion for a given cationic environment. Let us now analyse these cooperative effects in more detail:

Cationic effect: This effect corresponds to the influence of a chemical nature without any consideration for size or for geometrical phenomena since it is estimated for a given crystal lattice. For instance, in the poor cadmium region of the system, the large Cd^{2+} ions are locally subject to lattice constraints imposed by smaller Mg^{2+}, while reciprocally, the cadmium presence lead to relaxation effects for Cd^{2+}. However, they adopt the same local symmetry and one should consider only the cationic chemical intrinsic characteristics (e.g. effective charge, associated bond covalence, electronic configuration, polarizability…). As shown in Fig. 8, the chemical modification of the first shell through the substitution of x Mg^{2+} by x Cd^{2+} is accompanied by a ^{31}P shift of ~1.8, ~2.7, ~3.3 and ~3.5 ppm for $x = 1$, 2, 3 and 4, respectively. In that sense, it is remarkable that starting from the two border compounds, the shielding influence on the δ-^{31}P of Mg^{2+} for Cd^{2+} substitution is stronger than the de-shielding induced by Cd^{2+} introduction.

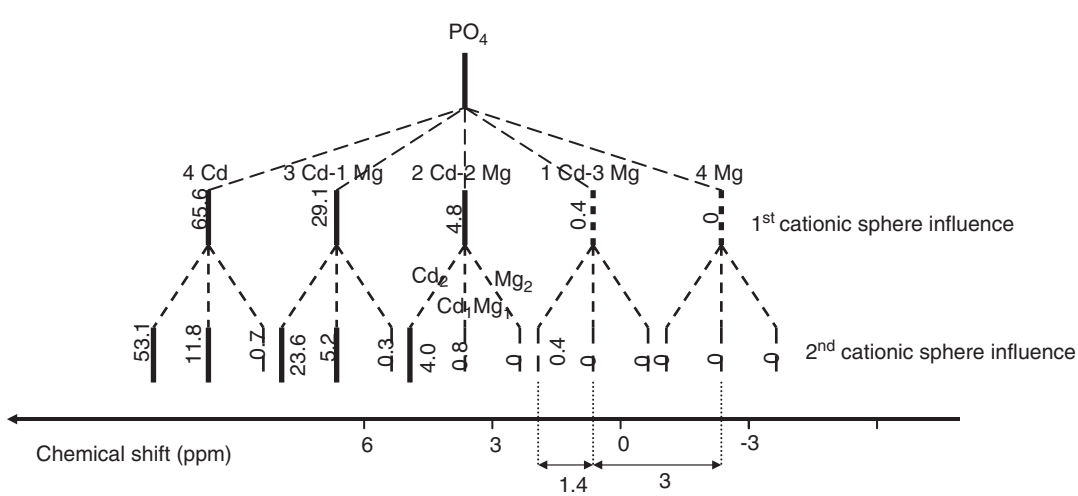

Fig. 7. Ideal scheme of the ^{31}P NMR spectrum for $BiMg_{0.2}Cd_{1.8}PO_6$ with evidence of the splits due to the first and second cationic coordination sphere. The theoretical weight (%) of each line is indicated. Lines with weight < 4% have not been considered in the fit. They are shown by dotted vertical lines.

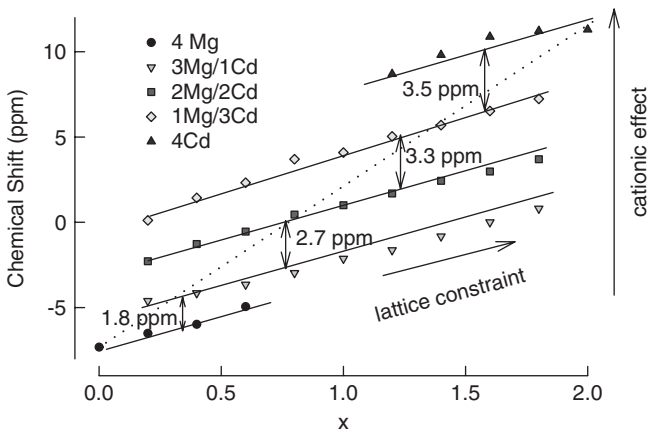

Fig. 8. Variation of the ^{31}P chemical shift for each possible configuration of first-neighbour cations against x. The full lines are to be used as a guideline.

Lattice constraints influence: The evolution of the ^{31}P chemical shift for a given surrounding cationic configuration represents the geometrical-only cationic influence. One should consider the strong unit cell dilatation occurring with x in $BiMg_{2-x}Cd_xPO_6$, in terms of an equilibrium obtained between constrained Cd^{2+} and relaxed Mg^{2+}. The resulting structural modifications (bond lengths, atomic and torsion angles,…) can be considered as lattice constraints. This influence is effective along the five lines plotted in Fig. 8. The linear variation of the ^{31}P chemical shift against x is estimated to be ca. 5 ppm throughout the solid solution. Therefore, it appears less drastic than the electric effect discussed above, i.e. ~11.5 ppm shift from a Mg-only to a Cd-only surrounding.

6. Concluding remarks

Through the structural and ^{31}P NMR analysis of selected $BiM_{2-x}M'_xPO_6$ systems, it has been shown that the neighbouring effect for the ^{31}P chemical shifts can be correlated to two independent influences, which are generally combined in the notion of Z/a^2 effective field. Therefore, it is possible to de-convolute the influence of the neighbouring cationic nature in terms of lattice constraints and the chemical nature effect. This has been possible using pertinent pairs of cations such as the Mg^{2+}/Cd^{2+} couple which is characterized by strong atomic displacements throughout the cationic substitution. In such a mixed system, each cation undergo the lattice effects imposed by the other chemical species, e.g. relaxations for the smaller Mg^{2+} and constraints for the larger Cd^{2+}, but still adopt identical local symmetries for a given compound. Thus, the correct assignment and analysis of the several ^{31}P resonances based on the distribution of cationic neighbours gave the means to clearly visualize the two correlated effects. Furthermore, the quantitative analysis of the resonances yields the verification of the statistic Mg^{2+}/Cd^{2+} distribution while diffraction experiments cannot fully reject the possibility of partial segregation in the crystal lattice. These results open a wide field of possible experiments and should give the opportunity to estimate the cationic role in a more detailed way. Of course, our analysis was possible considering the sensitive ^{31}P local probe well adapted to our study whereas other nuclei, like ^{51}V, would appear more problematic because of a strong anisotropic effect. In a similar fashion, the spectral resolution used here played a key-role in this work. Indeed, the full analysis of the $BiZn_{2-x}Mg_xPO_6$ system through NMR, for which similar Zn^{2+}/Mg^{2+} effects are expected, was not possible because of the weak effective chemical shift deviation.

Acknowledgments

The authors gratefully thank the Institut Laue Langevin, and particularly Dr. E. Suard for her help during neutron diffraction data aquisition. The FEDER, Région Nord Pas-de-Calais, Ministère de l'Education Nationale de l'Enseignement Supérieur et de la Recherche, CNRS and USTL are acknowledged for funding of NMR spectrometers.

Appendix A. Supplementary data

Supplementary data associated with this article can be found in the online version at doi:10.1016/j.jssc.2006.04.014.

References

[1] M. Huvé, M. Colmont, O. Mentré, Chem. Mater. 16 (2004) 2628.
[2] M. Ketatni, O. Mentré, F. Abraham, F. Kzaiber, B. Mernari, J. Solid State Chem. 139 (1998) 274.
[3] M. Ketatni, M. Huvé, F. Abraham, O. Mentré, J. Solid State Chem. 172 (2) (2002) 327.
[4] M. Colmont, M. Huvé, M. Ketatni, F. Abraham, O. Mentré, J. Solid State Chem. 176 (1) (2003) 221.
[5] M. Colmont, M. Huvé, F. Abraham, O. Mentré, J. Solid State Chem. 177 (11) (2004) 4149.
[6] J. Huang, Q. Gu, A.W. Sleight, J. Solid State Chem. 105 (1993) 599.
[7] F. Abraham, M. Ketatni, G. Mairesse, B. Mernari, Eur. J. Solid State Chem. 31 (1994) 313.
[8] F. Abraham, O. Cousin, O. Mentré, M. Ketatni, J. Solid State Chem. 167 (2002) 168.
[9] F. Abraham, M. Ketatni, Eur. J. Solid State Inorg. Chem. 32 (1995) 429.
[10] S. Nadir, J.S. Swinnea, H. Steinfink, J. Solid State Chem. 148 (1999) 295.
[11] X. Xun, S. Uma, A.W. Sleight, J. Alloys Compd. 338 (2002) 51.
[12] M. Ketatni, F. Abraham, O. Mentré, Solid State Sci. 1 (1999) 449.
[13] X. Xun, S. Uma, A. Yokochi, A.W. Sleight, J. Solid State Chem. 167 (2002) 245.
[14] A. Mizrahi, J.P. Wignacourt, H. Steinfink, J. Solid State Chem. 133 (1997) 516.
[15] M. Ketatni, B. Mernari, F. Abraham, O. Mentré, J. Solid State Chem. 153 (2000) 48.
[16] A. Mizrahi, J.P. Wignacourt, M. Drache, P. Conflant, J. Mater. Chem. 5 (1995) 901.
[17] W.A. Dollase, L.H. Merwin, A. Sebald, J. Solid State Chem. 83 (1989) 140.
[18] B. Badraoui, A. Bigi, M. Debbabi, M. Gazzano, N. Roveri, R. Thouvenot, Eur. J. Inorg. Chem. 2001 (2001) 1261.

[19] S.K. Kulshreshtha, O.D. Jayakumar, V. Sudarsan, J. Phys. Chem. Solids 65 (2004) 1141.
[20] R.J.B. Jakeman, A.K. Cheetam, N.J. Clayden, C.M. Dobson, J. Am. Chem. Soc. 107 (1985) 6249.
[21] Fullprof 2000, Rodriguez-Carvajal, Juan, Laboratoire Leon Brillouin (CEA-CNRS), 2000.
[22] D. Massiot, F. Fayon, M. Capron, I. King, S. Le Calvé, B. Alonso, J.-O. Durand, B. Bujoli, Z. Gan, G. Hoatson, Magn. Reson. Chem. 40 (2002) 70.
[23] R.D. Shannon, Acta Crystallogr. A 32 (1976) 751.
[24] I. Radosavljevic, A.W. Sleight, J. Solid State Chem. 149 (2000) 143.
[25] I. Radosavljevic, J.A.K. Howard, A.W. Sleight, Int. J. Inorg. Mater. 2 (2000) 543.
[26] N. Tancret, Ph.D. Thesis dissertation, Université des Sciences et Technologies de Lille, France, September 1995.
[27] G.L. Turner, K.A. Smith, R.J. Kirkpatrick, E. Oldfield, J. Magn. Res. 70 (1986) 408.
[28] A.K. Cheetham, N.J. Clayden, C.M. Dobson, R.J.B. Jakeman, J. Chem. Soc. Chem. Comm. (1986) 195.
[29] I. Abrahams, C. Christopher, J. Groombridge, Chem. Soc. Dalton Trans. (2000) 155.
[30] R.T. Sanderson, Polar Covalence, Academic Press, New York, 1983, p. 40.